

Millimeter-wave investigation of the antiferromagnetic phase in λ -(BETS)₂FeCl₄ in high magnetic fields

I. Rutel,¹ S. Okubo,² J. S. Brooks,¹ E. Jobiliong,¹ H. Kobayashi,³ A. Kobayashi,⁴ and H. Tanaka⁵

¹National High Magnetic Field Laboratory and Physics Department, Florida State University, Tallahassee, Florida 32310, USA

²Physics Department, Kobe University, Kobe, Japan

³Institute for Molecular Science, Okazaki, Japan

⁴Department of Chemistry, University of Tokyo, Tokyo 113, Japan

⁵Nanotechnology Research Institute and AIST, Tsukuba 305-8568, Japan

(Received 9 May 2003; published 29 October 2003)

The antiferromagnetic metal-insulator transition in the magnetic-organic conductor λ -(BETS)₂FeCl₄ has been probed by resonant cavity mm wave methods vs magnetic field, temperature, frequency, and sample orientation. Although the general form of the ac response follows expectations for passage from a skin depth regime to a depolarization regime as the metal-insulator phase boundary is crossed, additional features appear below the metal-insulator transition. This behavior indicates that metastable changes in the ground state occur within the insulating phase.

DOI: 10.1103/PhysRevB.68.144435

PACS number(s): 75.30.Kz, 76.30.-v, 76.50.+g

I. INTRODUCTION

The discovery of magnetic field induced superconductivity in λ -(BETS)₂FeCl₄ (Ref. 1) has drawn attention to the π - d electron spin-exchange mechanisms² in molecular systems where magnetic order in the d electron system strongly influences the behavior of the conducting π electron system. The more general λ -(BETS)₂Ga_{1-x}Fe_xBr_yCl_{4-y} class of organic conductors, with localized magnetic moments at the anion sites and conduction electrons in the molecular-cation layers exhibits competition between magnetic, metallic, insulating, and superconducting ground states.^{3,4} The magnetic-field-dependent phase diagram of the λ -(BETS)₂FeCl₄ material is shown in Fig. 1. For $H=0$, and below the metal-insulator transition temperature ($T_{MI} = 8.3$ K), λ -(BETS)₂FeCl₄ enters a highly insulating antiferromagnetic phase.⁵ Below T_{MI} , a spin-flop transition to a canted antiferromagnetic (CAF) phase occurs near 1 T, and above 11 T, a paramagnetic metallic (PM) phase appears. At higher magnetic fields (parallel to the conducting molecular planes), field-induced superconductivity (FISC) is stabilized below 5 K between 18 and 45 T.⁶ The FISC state involves the cancellation of the exchange field by the external magnetic field. Recent alloy studies on λ -(BETS)₂Ga_{1-x}Fe_xBr_yCl_{4-y} have given further support to this (Jaccarino-Peter) mechanism.⁴ Although the CAF-PM transition is nearly independent of field direction, the PM-FISC transition requires careful alignment of the field in the a - c molecular planes to avoid orbital dissipation in the superconducting phase.

In addition to the remarkable phenomena presented by the high-field FISC state, the low field, metallic and antiferromagnetic phases also present nontrivial behavior. Considerable attention has been given to the low-temperature ground state in the range 70 K to T_{MI} where anomalies in specific heat,⁷ NMR,⁸ and ac conductivity⁹ indicate the evolution of ferroelectric behavior. Additionally, below T_{MI} , antiferromagnetic magnetic resonance (AFMR) (Refs. 5 and 10) and

nonlinear conductivity¹¹ have been reported.

The purpose of the present work has been to explore various aspects of the phase diagram of λ -(BETS)₂FeCl₄ shown in Fig. 1 by way of mm wave perturbative cavity methods in the frequency range 40–100 GHz. For organic conductors, AFMR, electron-spin resonance (ESR), cyclotron resonance, and changes in complex conductivity are all in principle accessible under varying conditions of frequency, cavity mode, and sample orientation.^{10,12–16} Of direct relevance to the present work is the application of this method to metal-insulator transitions. Dressel *et al.*^{16,17} investigated T_{MI} ($= 133$ K) in α -(BEDT-TTF)₂I₃ between 10 and 600 GHz. For temperatures above T_{MI} , the sample is in the metallic

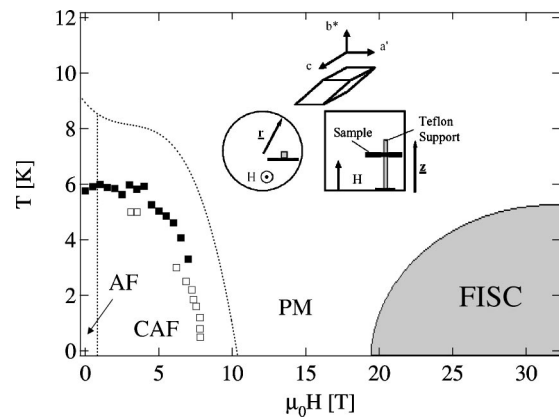


FIG. 1. Phase diagram of λ -(BETS)₂FeCl₄. The four phases identified are antiferromagnetic (AF), canted antiferromagnetic (CAF), paramagnetic metal (PM) (after Ref. 5), and field induced superconducting (FISC) (after Ref. 6). Closed (open) symbols represent the temperature (field) sweep measurements of the main depolarization feature observed in the CAF state for sample 1 from Figs. 2–3. Schematic: top figure, sample geometry and principle axes. Lower figures: axial and side views of sample orientation. The sample position shown is for the c axis $\parallel \hat{r}$ and the c axis $\perp \hat{z}$, where \hat{r} and \hat{z} are the unit directions for the axial and radial components of the cylindrical cavity.

state, but the skin depth was still greater than the sample thickness (i.e., the sample is in the depolarization regime). Below T_{MI} , the depolarization limit is reached as the sample becomes highly insulating. As the sample passes between these two limits, a sharp feature (the so-called depolarization peak) appears in both the frequency shift ($\Delta f/f_0$) and the line width ($\Delta\Gamma/2f_0$). In this case the sample was placed in the cavity with a TE_{011} mode such that the electric field was along the a axis of the crystal ($E\parallel a$). From $\Delta\Gamma/2f_0$ and $\Delta f/f_0$ one may compute the real parts of the ac conductivity and the dielectric constant ϵ_1 . Below T_{MI} , σ_{ac} was found to be significantly larger (four orders of magnitude at 60 GHz) than the dc conductivity, and σ_{ac} also increased with frequency. Also below T_{MI} , ϵ_1 was of the order of 20 in the 10-GHz range and increased with decreasing frequency. It was speculated that a collective mode may be responsible for this behavior. Matsui *et al.*,⁹ using the same type of ac electric-field configuration ($E\parallel a$, etc.), observed a similar type of depolarization peak in λ -(BETS)₂FeCl₄ at 16.3 GHz upon passage through T_{MI} . Below T_{MI} they also found that σ_{ac} was larger than σ_{dc} , again by several orders of magnitude, and ϵ_1 was of the order of 10.

II. EXPERIMENT

In our investigation of mm wave response of λ -(BETS)₂FeCl₄ in high magnetic fields, a mm wave resonant cavity perturbation method has been employed¹⁸ where the sample orientation in the cavity can be changed with respect to the field orientation. Because we were interested in probing the general response with field and temperature, the sample placement was such that both ac magnetic H_{ac} and electric E_{ac} fields radiated the sample. In Fig. 1 the convention for orientation is given in terms of the principle axes of the crystal, and the radial and axial ($\hat{z}\parallel\vec{H}$ in all cases) unit vectors associated with the cavity. The center of mass of the sample was always approximately 1/3 of the cavity height, and 2/3 out along the cavity radius. Samples were synthesized by electrochemical methods.¹⁹ Two single crystals were used for two independent measurements in this work. Sample 1 was $0.97\times 0.10\times 0.10$ mm³ in size and sample 2 (only studied for one orientation) was $0.50\times 0.15\times 0.05$ mm³ in size. From the temperature-dependent resistivity,¹¹ we find the skin depth above T_{MI} to be of the order of 10 μ m in the range 60–100 GHz, and below T_{MI} at 4 K, the skin depth rises to almost 10 mm in the same frequency range. The filling factor is of the order of 10^{-5} . From values of the Dingle temperature ($T_D=0.5$ K) determined from Shubnikov–de Haas measurements in the metallic state²⁰ we estimate the mean free path and relaxation time in the a - c conducting planes to be of the order of 10 μ m and 1.0×10^{-10} s, respectively. Samples were greased to a small teflon mount inside the cylindrical cavity resonator. A control experiment ensured that the grease and teflon support did not contribute a significant background or spurious ESR signal. In all cases, data were taken in the phase-locked mode, and the amplitude and frequency of the cavity response were recorded for either fixed temperature or fixed magnetic field. Resonant cavity Q 's were typically in the range of 5000–

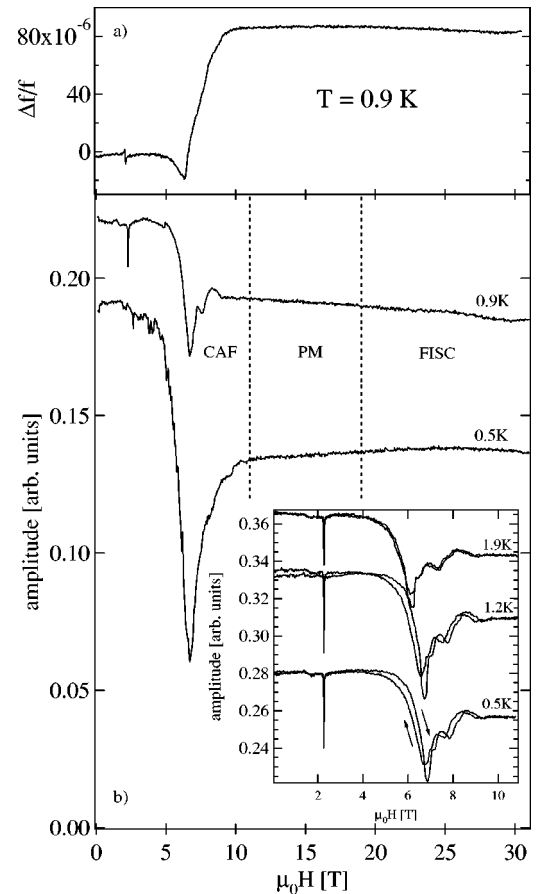


FIG. 2. Low-temperature ($T < T_{MI}$) field-dependent mm wave cavity response of λ -(BETS)₂FeCl₄ for $c\parallel\hat{z}$, $c\parallel\vec{H}$, $\nu=66.9$ GHz (for 0.9 K), $\nu=75.4$ GHz (for 0.5 K). (a) Frequency change for the phase-locked 66.9-GHz data at 0.9 K. (b) Cavity amplitude response. The sharp dip near 2 T is the ESR line, the first large dip near 6 T is the depolarization peak, and the features at higher fields are related to metastable structure within the CAF phase. Although the sample was aligned to allow the high-field superconducting (FISC) state to be stabilized, only weak features associated with a metal to superconducting transition were detected. Inset: Full field sweeps to 12 T for 66.9 GHz (done in a lower field magnet after thermal cycling). Hysteresis is observed in the depolarization and metastable structure in the CAF state.

10 000. Experiments were carried out in a 30-T resistive magnet and an 8-T superconducting magnet where either temperature or field was held fixed at a specific resonant cavity mode frequency. A helium three-probe was modified to allow temperatures down to 0.5 K without interference from liquid dielectric effects.

III. RESULTS AND DISCUSSION

Our results are presented in Figs. 2–4 and 6 for sample 1 and in Fig. 5 for sample 2. Representative results for the resonant cavity amplitude are shown for magnetic field sweeps in Fig. 2 for $c\parallel\hat{z}$ for several temperatures below T_N up to 30 T. Also shown is the change in frequency for the 66.9 GHz trace at 0.9 K: here the signal is the phase-locked

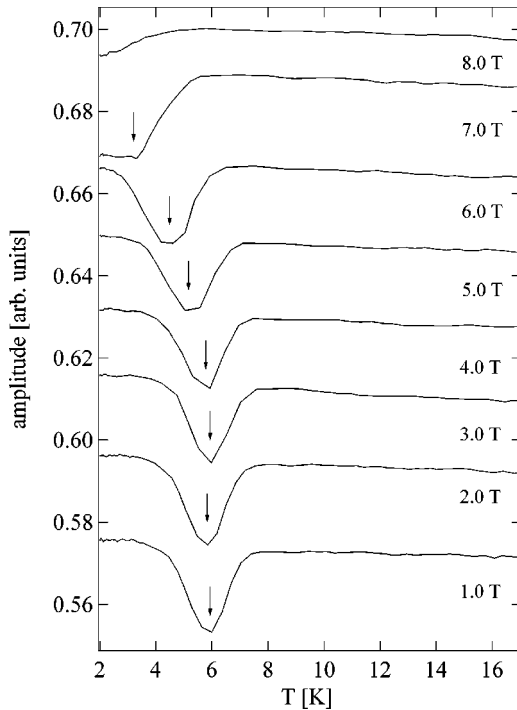


FIG. 3. Temperature dependence of the cavity response at different fields for λ -(BETS) $_2$ FeCl $_4$; $c \parallel \vec{H}$, $a \parallel \hat{r}$, $\nu = 64.927$ GHz, for sample 1. The temperature dependence of the main depolarization feature is marked by arrows, and is also plotted in Fig. 1.

amplitude of the cavity response, where resonant frequency is allowed to change (via feedback) to keep the phase reference in quadrature. The behavior of $\Delta f/f$ closely follows the functional form of the depolarization behavior.^{14–16} Here however, it is the magnetic field that is changing the resistivity (by many orders of magnitude, from an insulator to a conductor), and thereby the skin depth over an equally large range of values. The general form of the mm wave cavity response for magnetic field sweeps below T_{MI} involved several signals. At low fields (below 5 T and below T_{MI}) we observed the ESR and AFMR signals (Figs. 2, 4–6) due to the magnetic resonant condition (i.e., $h\nu = g\mu_B B$) for electron spin. Here the resistivity is very high and the material is in the depolarization limit. For further increases in field (or temperature—see Ref. 21), the resistivity begins to decrease and at the CAF-PM phase boundary the sample returns to a metallic state. From the sample and cavity parameters given above, we expect the sample, near and above T_{MI} , to be intermediate between the skin depth and depolarization conditions, as well as between Hagen-Rubens ($\omega\tau < 1$) and relaxation ($\omega\tau > 1$) regimes.¹⁴ Hence as the metallic phase boundary is approached from within the CAF phase, the sample exhibits a depolarization peak behavior, as indicated by the sharp dip in both the resonant amplitude and frequency (Fig. 2). At fields between the depolarization peak and the CAF-PM boundary, additional structure in the ac response is observed, and at lower temperatures hysteresis appears in the data. When studied systematically with temperature (inset of Fig. 2), the depolarization peak and the additional structure follow the temperature dependence of

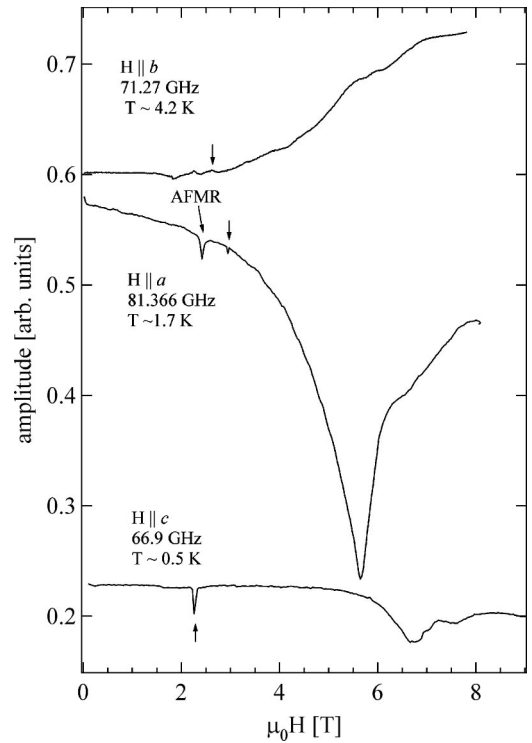


FIG. 4. Comparison of the magnetic field dependence of cavity response for λ -(BETS) $_2$ FeCl $_4$ for three different sample orientations, frequencies, and temperatures. Arrows indicate the position of the ESR lines and the AFMR line for $a \parallel \vec{H}$ is also indicated. The details of the depolarization structure above 4 T are dependent on sample orientation and frequency.

the CAF-PM phase boundary. The temperature dependence of the depolarization peak at fixed field has also been investigated for sample 1, as shown in Fig. 3. As the CAF phase is entered from higher temperatures, the signal is observed to fall, then to rise and approach a value higher than that observed above T_{MI} . The T - H plot of these features (shown in Fig. 1) follows the general shape of the CAF-PM phase boundary.

In contrast to previous studies⁹ (where the sample is placed in the maximum of the ac electric field), we do not find sharp changes in the cavity response at T_{MI} (along the CAF-PM phase boundary). We attribute this to our sample configuration, which experiences both ac magnetic and electric fields. Moreover, we do see a sharp feature at the PM-FISC boundary, but only a gradual change as the FISC state is entered as is indicated in Fig. 2 for the 66.9-GHz data. This may be due in part to the sample orientation, since the FISC state is very sensitive to sample alignment and we cannot change the position *in situ*. In addition, for mm wave studies, the metal-to-type II superconductor transition does not involve a rapid change (jump) in the surface impedance,²² and this will likewise preclude any large differences (jumps) in the cavity response as the FISC state is entered.

The depolarization peak and the metastable structures are dependent on sample orientation and frequency, as shown in Fig. 4. Here the sample was measured for three different field

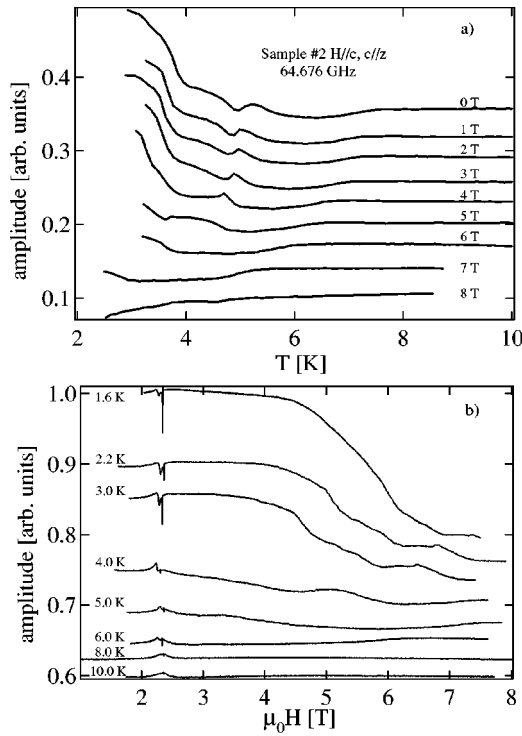


FIG. 5. mm wave cavity response of sample 2 at 64.676 GHz for $H||c, c||\hat{z}$. (a) Temperature dependence for constant field values. (b) Field dependence for constant temperatures. Sharp dips are from a diphenylpicrylhydrazyl marker and broader dips at slightly lower fields are due to the ESR line from the sample.

orientations, frequencies, and temperatures. The ESR line is prominent and absorptive at two of the frequencies, and for $c||\hat{r}, a||\vec{H}$ the AFMR signal is observed. (Strong ESR or AFMR signals are good indications of the sample's coupling to \vec{H}_{ac} .) In contrast, the ESR line is weak for the 71.27-GHz data and the field dependence of the background is reversed. It is apparent that the overall signal depends on how the sample is coupled with an \vec{E}_{ac} or \vec{H}_{ac} excitation mode, as indicated by the intensity of the ESR features. However, the ESR line positions rigorously follow the linear frequency dependence, as presented in Fig. 6 below.

To check the sample dependence of the depolarization and metastable behavior, we investigated a second sample (2) in an 8-T magnet. The temperature- and field-dependent data are shown in Fig. 5. This sample, which was partially twinned, was smaller than the first, and was only studied for $c||\vec{H}||\hat{z}$ and for 64.7 GHz. In both the field and temperature dependence, the depolarization effect, as well as additional structure in the response, is observed. Although the features follow the general T - H dependence of the CAF-PM phase boundary, the details of the signals of samples 1 and 2 are different. In particular, the field dependence of sample 2 (compared with sample 1) does not show a sharp depolarization dip, but it does have considerably more structure in the temperature dependence. We attribute the differences in the behavior of two samples to details of the sample geometry (shape, twinning) and cavity mode (resonant frequency) factors.

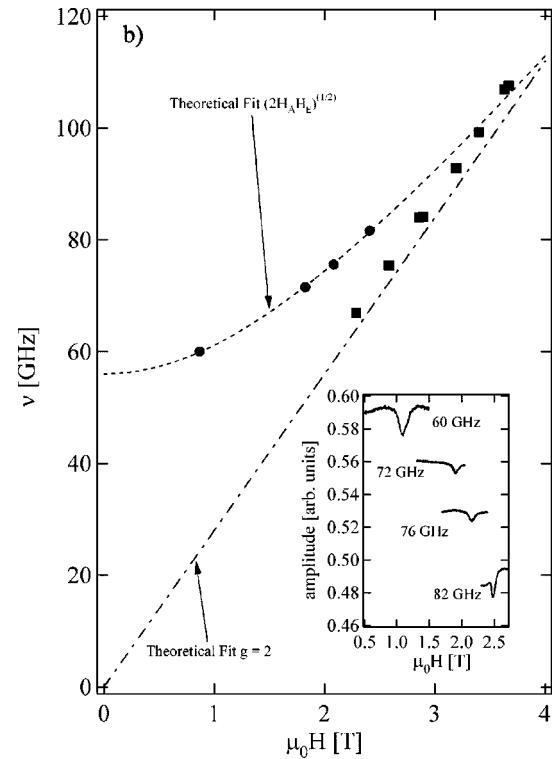
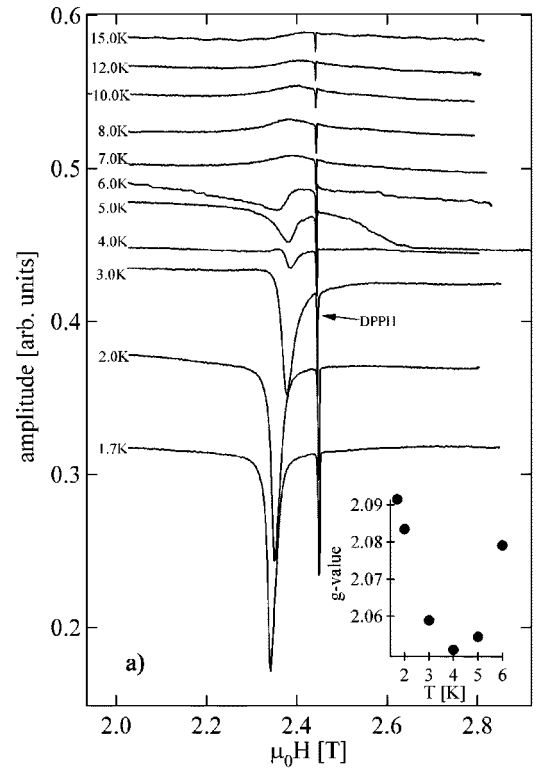


FIG. 6. (a) Detailed temperature dependence of the ESR line (with respect to the diphenylpicrylhydrazyl marker); $a||\hat{r}, c||\vec{H}, \nu = 66.9$ GHz. Below T_{MI} the g factor is nonmonotonic with decreasing temperature. Inset: detail of temperature-dependent g factor below T_{MI} . (b) AFMR and ESR frequency dependence. Solid circles—AFMR vs frequency for $c||\hat{r}, a||\vec{H}$. Solid squares—ESR vs frequency for $c||\hat{z}, c||\vec{H}$. Inset: detail of AFMR frequency dependence.

The frequency dependence of the ESR and the AFMR signals were investigated for $c\|\hat{z}$, $c\|\vec{H}$ and $c\|\hat{r}$, $a\|\vec{H}$, respectively, as shown in Fig. 6. For field directions away from the hard axis (see below), only the ESR line is observed. Below T_{MI} there is a nonmonotonic change in the g factor with temperature, indicating that the CAF state is still developing, even at low temperatures. The first observation of AFMR in λ -(BETS) $_2$ FeCl $_4$ was reported by Brossard *et al.*⁵ in the X band for fields tilted with respect to the c axis along the a - b axes (called u in Ref. 5 due to the uncertainty in the a and b directions). They observed characteristic AFMR behavior, with the expected “bubble shape” for two resonant fields vs orientation. The higher field resonance (1.2 T) was only weakly temperature dependent, while the lower field resonance increased significantly below T_{MI} . In a more recent study¹⁰ AFMR was investigated for a dc magnetic field tilted about 30° away from c towards b . Here two resonances again appear as in Ref. 5, but the higher resonance (1.3 T), also weakly temperature dependent, was attributed to the spin-flop transition, and not to AFMR. The lower resonance was temperature dependent, and increased with decreasing temperature. For the field along the a axis, also measured in Ref. 10, a single AFMR line is seen, which is both temperature and frequency dependent. This configuration, $\vec{H}\|a$, corresponds to our investigation, as shown in Fig. 6. For the orientation $a\|\vec{H}$, $c\|\hat{r}$, we measured the field position of the AFMR signal over our accessible range of frequency (~ 40 –110 GHz), as plotted in Fig. 6(b) (also shown is a representative trace of data for $a\|\vec{H}$, $c\|\hat{r}$ in Fig. 4). The frequency-field dependence of the AFMR signal is consistent with the field orientation along the hard axis of the sample,^{23–26} indicating that the hard axis is along a , as previously reported.¹⁰ An extrapolation of the AFMR to zero field gives a gap frequency corresponding to a characteristic field of 1.7 T. This value, which is related to the product of the exchange field and the anisotropy field, is comparable to the spin-flop fields (1.1 T–1.3 T) reported in both magnetization and other ESR studies. A linear fit of the ESR line yields a g value of 2.05 for sample orientations away from $a\|\vec{H}$.

IV. SUMMARY

In summary, we have used mm wave perturbative cavity methods in a generalized, nonspecific H_{ac} and E_{ac} configuration to explore the characteristics of the λ -(BETS) $_2$ FeCl $_4$ field-temperature phases. A rapid change in the resistivity of the sample below the antiferromagnetic ordering temperature at T_{MI} leads to the appearance of a depolarization behavior in the cavity response. However, we observe additional features in the response below T_{MI} which indicate that the electrodynamic properties of the material encounter metastabi-

lites (as also seen in resistance measurements). Both the depolarization peak and the metastable features (which are reproducible with temperature and magnetic field for a given sample) follow the general temperature-field dependence of the CAF state. It is notable that the ac conductivity observed below T_{MI} in previous microwave studies^{9,16,17} can be orders of magnitude higher than the dc conductivity. This may be part of the reason that the mm wave cavity response is sensitive to metastable changes in the CAF ground state below T_{MI} , even though the dc resistivity is large. The origin of the metastability, as previously noted in resistance measurements,²⁷ is at present unknown. However, we may speculate that it is related to the unique nature of the physically separated p -electron cation and d -electron anion layers, together with the large d - d and π - d interactions that are expected to be present.² Brossard *et al.* have previously considered the Ruderman-Kittel-Kasuya-Yosida interaction between the Fe $^{3+}$ and spin- $\frac{1}{2}$ conduction electron spins.⁵ Here they predicted the possibility of a sequence of different canting angles as the PM phase was approached. Such a process might lead to domainlike structures as increasing field destroys the CAF state. Hysteresis in the lower temperature data, as is evident in Fig. 2, is suggestive of domain-type behavior. In preliminary magnetization studies, we have observed precursor structure in the susceptibility as the CAF-PM phase boundary is approached with increasing field, indicating that the thermodynamic state of the system is changing significantly.²⁹ Similarly, hysteretic behavior in the magnetization near the CAF-PM phase boundary has been reported in previous magnetization studies.⁵ As in previous measurements, we observe the antiferromagnetic resonance for the dc magnetic field parallel to the hard (a) axis. Its frequency dependence yields the spin-flop field (about 1.2 T). As the PM-FISC state is crossed, only a weak change in the cavity response is observed. In light of this, higher frequency studies in the range 1 THz would be highly desirable to explore changes in the ESR line due to the expected cancellation of the exchange field²⁸ near the center of the FISC phase.

ACKNOWLEDGMENTS

We are grateful to S. Wieggers, J. Rook, and H. van Luong for allowing us to use the new Nijmegen-Amsterdam Magnet Laboratory resistive magnet prior to formal commissioning, and to S. Hill and N. Toyota for useful discussions. S.O. acknowledges support from Venture Business Laboratory, Kobe University. This work was supported by Grants Nos. NSF-DMR 99-71474 and 02-03532. The mm wave facility is supported through Grant No. NHMFL/IHRP 5042, and the NHMFL is supported by a contractual agreement between the NSF and the State of Florida.

- ¹S. Uji *et al.*, Nature (London) **410**, 908 (2001).
- ²T. Mori and M. Katsuhara, J. Phys. Soc. Jpn. **71**, 826 (2002).
- ³H. Tanaka, H. Kobayashi, A. Kobayashi, and P. Cassoux, Adv. Mater. (Weinheim, Ger.) **12**, 1685 (2000), and references therein.
- ⁴S. Uji, C. Terakura, T. Terashima, T. Yakabe, Y. Terai, Y. Imanaka, S. Yasuzuka, M. Tokumoto, F. Sakai, A. Kobayashi, H. Tanaka, H. Kobayashi, L. Balicas, and J.S. Brooks, J. Phys. Soc. Jpn. **72**, 369 (2003).
- ⁵L. Brossard, R. Clerac, C. Coulon, M. Tokumoto, T. Ziman, D.K. Petrov, V.N. Laukhin, M.J. Naughton, A. Audouard, F. Goze, A. Kobayashi, H. Kobayashi, and P. Cassoux, Eur. Phys. J. B **1**, 439 (1998).
- ⁶L. Balicas, J.S. Brooks, K. Storr, S. Uji, M. Tokumoto, H. Tanaka, H. Kobayashi, A. Kobayashi, V. Barzykin, and L.P. Gor'kov, Phys. Rev. Lett. **87**, 067002 (2001).
- ⁷E. Negishi, H. Uozaki, Y. Ishizaki, H. Tsuchiya, S. Endo, Y. Abe, H. Matsui, and N. Toyota, Synth. Met. **133-134**, 555 (2003).
- ⁸S. Endo, T. Goto, T. Fukase, H. Matsui, H. Uozaki, H. Tsuchiya, E. Negishi, Y. Ishizaki, Y. Abe, and N. Toyota, Synth. Met. **133-134**, 557 (2003).
- ⁹H. Matsui, H. Tsuchiya, E. Negishi, H. Uozaki, Y. Ishizaki, Y. Abe, S. Endo, and N. Toyota, J. Phys. Soc. Jpn. **70**, 2501 (2001).
- ¹⁰T. Suzuki, H. Matsui, H. Tsuchiya, E. Negishi, K. Koyama, and N. Toyota, Phys. Rev. B **67**, 020408(R) (2003).
- ¹¹N. Toyota, Y. Abe, H. Matsui, E. Negishi, Y. Ishizaki, H. Tsuchiya, H. Uozaki, and S. Endo, Phys. Rev. B **66**, 033201 (2002).
- ¹²S. Hill, N.S. Dalal, and J.S. Brooks, Appl. Magn. Reson. **16**, 237 (1999).
- ¹³S. Hill, J. Brooks, Z. Mao, and Y. Maeno, Phys. Rev. Lett. **84**, 3374 (2002), and references therein.
- ¹⁴O. Klein, S. Donovan, M. Dressel, and G. Gruner, Int. J. Infrared Millim. Waves **14**, 2423 (1993).
- ¹⁵S. Donovan, O. Klein, M. Dressel, K. Holczer and G. Gruner, Int. J. Infrared Millim. Waves **14**, 2459 (1993).
- ¹⁶M. Dressel, O. Klein, S. Donovan, and G. Gruner, Int. J. Infrared Millim. Waves **14**, 2489 (1993).
- ¹⁷M. Dressel, G. Gruner, J.P. Pouget, A. Breining, and D. Schweitzer, J. Phys. I **4**, 579 (1994).
- ¹⁸M. Mola, S. Hill, P. Goy, and M. Gross, Rev. Sci. Instrum. **71**, 186 (2000).
- ¹⁹A. Kobayashi, T. Udagawa, H. Tomita, T. Naito, and H. Kobayashi, Chem. Lett. **1993**, 2179 (1993).
- ²⁰S. Uji, H. Shinagawa, C. Terakura, T. Terashima, T. Yakabe, Y. Terai, M. Tokumoto, A. Kobayashi, H. Tanaka, and H. Kobayashi, Phys. Rev. B **64**, 024531 (2001).
- ²¹J.S. Brooks, L. Balicas, K.A. Storr, H. Kobayashi, H. Tanaka, A. Kobayashi, S. Uji, and M. Tokumoto, Synth. Met. **133-134**, 485 (2003).
- ²²M. Dressel, S. Bruder, G. Gruner, K.D. Carlson, H.H. Wang, and J.M. Williams, Phys. Rev. B **48**, 9906(R) (1993).
- ²³S. Foner, Phys. Rev. **107**, 683 (1957).
- ²⁴M. Hagiwara and K. Katsumata, RIKEN Rev. **24**, 12 (1993).
- ²⁵C. Coulon, J. C. Scott, and R. Laversanne, Phys. Rev. B **33**, 6235 (1986).
- ²⁶J.B. Torrance, H.J. Pedersen, and K. Bechgaard, Phys. Rev. Lett. **49**, 881 (1982).
- ²⁷H. Matsui, H. Tsuchiya, and N. Toyota, J. Phys. Soc. Jpn. **71**, 668 (2002).
- ²⁸O. Cepas, R.H. McKenzie, and J. Merino, Phys. Rev. B **65**, 100502(R) (2002).
- ²⁹D. Graf, J.S. Brooks, E.S. Choi, H. Tanaka, M. Tokumoto, H. Kobayashi, and A. Kobayashi (unpublished).